Plasma Oscillation Effects on Nested Hall Thruster Operation and Stability

Michael S. McDonald
Aerospace Engineering
University of Michigan
Ann Arbor, MI 48109
734-764-4199
msmcdon@umich.edu

Michael J. Sekerak
Aerospace Engineering
University of Michigan
Ann Arbor, MI 48109
734-764-4199
msekerak@umich.edu

Alec D. Gallimore
Aerospace Engineering
University of Michigan
Ann Arbor, MI 48109
734-764-8224
alec.gallimore@umich.edu

Richard R. Hofer
Jet Propulsion Laboratory
California Institute of Technology
Pasadena, CA 91109
818-393-2506
richard.r.hofer@jpl.nasa.gov

Abstract—**High-power Hall thrusters capable of throughput on the order of 100 kW are currently under development, driven by more demanding mission profiles and rapid growth in on-orbit solar power generation capability. At these power levels the nested Hall thruster (NHT), a new design that concentrically packs multiple thrusters into a single body with a shared magnetic circuit, offers performance and logistical advantages over conventional single-channel Hall thrusters. An important area for risk reduction in NHT development is quantifying inter-channel coupling between discharge channels. This work presents time- and frequency-domain discharge current and voltage measurements paired with high-speed video of the X2, a 10-kW class dual channel NHT. Two "triads" of operating conditions at 150 V, 3.6 kW and 250 V, 8.6 kW were examined, including each channel in individual operation and both channels in joint operation. For both triads tested, dual-channel operation did not noticeably destabilize the discharge. Partial coupling of outer channel oscillations into the inner channel occurred at 150 V, though oscillation amplitudes did not change greatly. As a percentage of mean discharge current, RMS oscillations at 150 V increased from 8% to 13% on the inner channel and decreased from 10% to 8% on the outer channel from single- to dual-channel operation. At 250 V the RMS/mean level stayed steady at 13% on the inner channel and decreased from 7% to 6% on the outer channel. The only mean discharge parameter noticeably affected was the cathode floating potential, which decreased in magnitude below ground with increased absolute cathode flow rate in dual-channel mode. Rotating spokes were detected on high-speed video across all X2 operating cases with wavelength 12-18 cm, and spoke velocity generally increased from single- to dual-channel operation.**

Table of Contents

978-1-4673-1813-6/13/$31.00 ©2013 IEEE.
[1] IEEEAC Paper #2502, Version 3, Updated 06/01/2013.

1. Introduction

Several factors have driven the development of high-power Hall thrusters in the several tens of kilowatts in the past decade. First is the growing availability of electric power on orbit. Over the past 40 years spaceborne solar power generation capability has followed a roughly exponential growth curve, doubling every four years. This trend is on pace to demonstrate spaceborne solar arrays with power levels on the order of 100 kW - 1 MW by 2020.[1] Recent examples of research enabling continuation of this trend are the DARPA Fast Access Spacecraft Testbed (FAST) program, which was aimed at development of 50-80 kW onboard solar power generation capability,[2] and further development under the Boeing Integrated Blanket Interconnect System (IBIS) 30-kW program.[3], [4] The second is the sharp improvement in electric propulsion (EP) mission trip times possible with increased acceleration at higher power, motivating development of EP systems capable of taking advantage of the increasing power availability.[5] A third factor is the high technological maturity of high-power Hall thrusters compared to other EP devices potentially scalable to high power, including ground testing demonstration to 72 kW in the NASA-457Mv1 a decade ago[6] and high-efficiency, high-I_{sp} operation demonstrated in excess of 3000 s on the NASA-173Mv2 a few years later. [7]

Near- to mid-term EP power throughput requirements for the Air Force have been estimated at 100 - 200 kW,[5] while near-term missions of interest to NASA are on the order of 300 kW for near-earth asteroid (NEA) targets[1] and 300-700 kW for missions to Mars or the Martian moons.[8] While this is an admittedly wide span of power, a recently developed mass and cost model for thruster sizing in EP missions indicated wide latitude for mission planners in selecting thruster power level to meet both power throughput and mission redundancy requirements, and indicated that development of a baseline "low"-power thruster in the 20-50 kW range and a high-power 50-100 kW thruster would be optimum to support missions in the 200-500 kW and 500 kW-1 MW ranges, respectively.[9]

Somewhere within the 50-100 kW power level conventional single-channel Hall thrusters become unwieldy in size and fabricability, and the nested Hall thruster (NHT) begins to come into its own. The NHT is a compact Hall thruster design that incorporates two or more concentric Hall thruster channels into a single structure. At equivalent power density, this configuration offers significant advantages in thruster footprint, power scalability and throttling range at high efficiency compared to traditional, single-channel thrusters.[5], [10] Two NHTs are currently under active test or development, the X2 dual-channel and X3 triple-channel thrusters, both designed under support from the Air Force Research Laboratory (AFRL), with additional design input and support from NASA Glenn Research Center (GRC) and the Jet Propulsion Laboratory (JPL). [11], [12], [13], [14], [15]

In a design study comparison between the X3 NHT operating at 200 kW and a cluster of three NASA 457Mv1's with equal total power, shared components and better packing reduce the power-specific mass (kg/kW) of the NHT by 60% and the physical footprint by 50% compared to the cluster.[5] The NHT also extends the Hall thruster throttling range from 20-40X for single-channel thrusters to 100X for a dual-channel configuration, and 200X for a triple-channel configuration.[14] Finally, the NHT spans this wide range of power at much better efficiency than a single channel thruster by optimizing successive channel designs for staggered power levels. Rather than operate all channels at an off-design power level, channels are selectively turned on or off based on power level to maintain all channels at or near their design power density. Furthermore, NHT thruster and efficiency in multi-channel operation has been confirmed to exceed a simple superposition of individual channel performance characteristics due to beneficial coupling between the discharges.[12]

2. Motivation for NHT Coupling Investigations

While a number of the above features make the NHT concept attractive, a key area for risk reduction to advance the NHT beyond its current technology readiness level (~TRL-3) is in identifying consequences of inter-channel discharge coupling during multi-channel operation. Discharge coupling refers to differences between observed multi-channel NHT operation and simple superposition of measured single-channel operating characteristics. The enhanced thrust and efficiency in multi-channel NHT operation noted above is clearly a benefit of coupling, similar to that observed with conventional clusters, but other phenomena such as shared discharge oscillation frequencies across multiple channels in a NHT have also been observed.[12] There are potential risks from coupling including amplified discharge oscillations, unanticipated performance degradation, or increased erosion. The potential for interaction between oscillations, instabilities, or other time-resolved behaviors between channels is particularly challenging to address analytically because the nature of their interaction even in single-channel Hall thrusters is not well understood, though it does appear to be associated with strong transitions in thruster operating behavior.

Hall Thruster Oscillatory Modes

Several different oscillatory phenomena occur in a Hall thruster discharge,[16] most notably the breathing and rotating spoke modes. The Hall thruster breathing mode is a 5-35 kHz oscillation that has been variously linked to a predator-prey cycle between electrons and neutrals[17] and axial oscillation of the ionization zone inside the thruster discharge channel.[18] The mode gets its name from a simple description: the thruster "breathes in" neutrals from the injector, depletes them by electron impact ionization, "breathes out" the resulting ions and then waits for neutrals to refill the discharge channel to start anew.

Rotating spokes are azimuthally (i.e., around the discharge channel like a race-track) propagating waves that travel at a velocity well below the critical ionization velocity of the propellant gas, about 4 km/s in xenon.[19] Recent observations have confirmed that rotating spokes, largely neglected or undetected since early work on Hall thrusters in the 1960s and 70s, are still present even in modern high-power devices and have recently been detected by a variety of diagnostics, primarily high-speed imaging but also with azimuthally segmented anodes and Langmuir probes.[20], [21], [22], [23], [24], [25], [26] Both modes are associated with ionization, suggesting a potential for these modes to interact – perhaps for one wave structure to starve the other, or resonate with it, producing some manner of unexpected result. While the physics generating each mode is not perfectly understood (in the case of spokes, it is hardly understood at all), and the physics of such an interaction are thus not tractable analytically, transitions in Hall thruster operation have been observed and associated with changes in the relative strength of these two modes.

Transitions in Thruster Operating Condition

The first evidence of this behavior, the so-called Brown transition, was observed at low voltage in the H6 6-kW Hall thruster. While operating in a range from 100-120 V, relatively minor changes in thruster operating parameters such as magnetic field strength, test facility background pressure, cathode flow rate, or auxiliary neutral flow near the cathode were observed to trigger sudden visible changes in plume structure as well as drops in thruster efficiency of several percent and increases in mean discharge current oscillations from ~10% to ~100% of the mean discharge current.[27] Brown also noted that the transition occurred at higher discharge voltages as facility background pressure was reduced, suggesting that these transitions from stable, efficient operation to highly oscillatory, inefficient operation may occur near standard Hall thruster operating voltages in flight Hall thrusters given the much lower background pressure on orbit. Such a transition could manifest as an operating condition observed to be stable during ground testing becoming unstable in flight. Later investigation of the Brown transition in the H6 detected clear changes in the presence and coherence of rotating spoke modes in the discharge between high-efficiency and low-efficiency operation. More coherent or stronger spoke structures were associated with improved efficiency and reduced discharge current oscillation amplitude.[24] One hypothesis is that the spoke modes temper or damp the breathing mode. However, whether the spokes cause, are caused by, or are merely correlated with the reduced breathing mode through some hidden process is not clear, and needs further study.

Illustrating this lack of clarity, while in the H6 stronger spokes were associated with reduced mean discharge current, reduced discharge current oscillations and improved thrust and efficiency, another experiment using passive feedback to *diminish* spoke levels in the discharge of a cylindrical Hall thruster (CHT) *also* observed decreases in mean discharge current (thrust was not monitored).[28] It is not clear if the same physics are at play in the CHT as with annular thrusters, but in either case the presence or lack of spokes in the discharge is clearly linked with changes in thruster operation. Assuming that these two modes interact, then the situation rapidly becomes more complicated with multiple channels. In a thruster with N channels the number of potential breathing/spoke interactions goes as N^2. Adding to the list of potential interaction phenomena, in a nested Hall thruster adjacent channels have opposite magnetic field

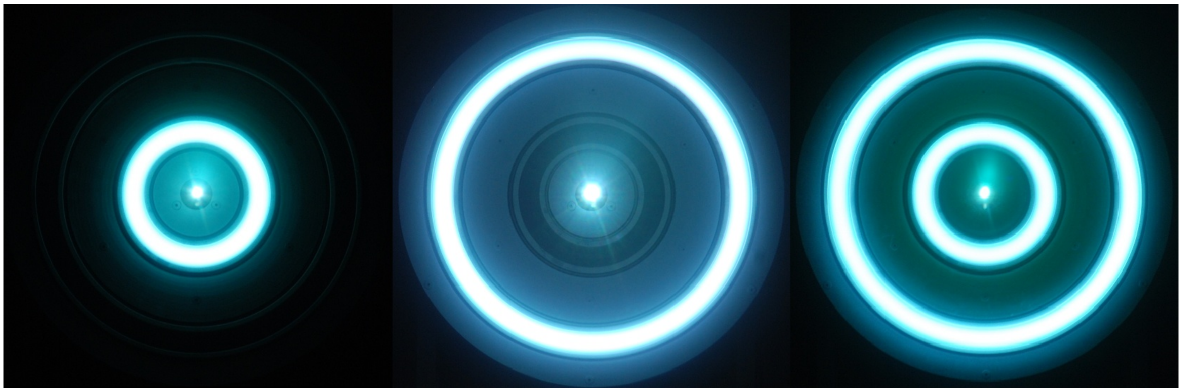

Figure 1. The three operational conditions possible for a dual-channel nested Hall Thruster (NHT). The left two cases show single channel operation with the inner and outer channels, respectively, while the far right shows dual channel operation. Under certain conditions these three cases form a "triad" of operating conditions (see Section 3).

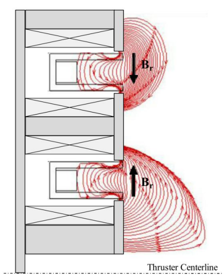

Figure 2. A typical magnetic field topography for a dual-channel NHT. The opposing directions of B_r in each channel due to the shared components of the magnetic circuit drive counter-rotating spokes in each channel of the NHT discharge. Figure courtesy of Brown.

polarity (Figure 2). Since spokes rotate in the $E \times B$ direction, spoke counter-rotation in adjacent channels of a NHT is expected and has been observed.[24] Thus, in addition to the chance for resonant instability, $E \times B$ shear may disrupt otherwise stable spoke rotation in another potential instability mechanism.

Goals of NHT Coupling Investigation

This investigation presents time-resolved observations of NHT operation with a focus on quantifying changes in discharge current and voltage oscillation frequencies and amplitudes during the transition from single- to dual-channel operation. High-speed imaging also quantifies changes in rotational instabilities in the discharge channel known as rotating spokes. The goal is to identify whether or not dual-channel operation promotes increased oscillation amplitudes, shared oscillation frequencies, or other phenomena that would tend to destabilize the thruster when moving from single- to dual-channel operation.

Additionally, the results presented here are part of a broader study investigating X2 time-resolved behavior using a combination of high-speed imaging and time-resolved Langmuir probes in the plasma plume for mapping of plasma properties and comparing the X2 to a high-performance single-channel thruster, the H6, at nearly matched operating conditions. A companion paper presents preliminary Langmuir probe results in the H6, though the comparison between the two thrusters is still underway.[29]

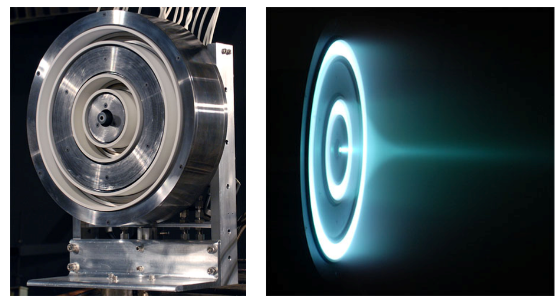

Figure 3. The 10-kW class X2 nested-channel Hall thruster (NHT), a dual-channel Hall thruster designed, built and tested at the University of Michigan Plasmadynamics and Electric Propulsion Laboratory (PEPL).

3. Experimental Equipment

Vacuum Facility

All experiments were conducted in the Large Vacuum Test Facility (LVTF) in the Plasmadynamics and Electric Propulsion Laboratory (PEPL) at the University of Michigan. The LVTF is a stainless steel-clad vacuum chamber 9 m long and 6 m in diameter, with an approximate volume of 200 m^3. The chamber was originally built in 1961 by the Bendix Corporation as a space simulation chamber with thermal testing capability and was donated to the University of Michigan in the 1980s. It is brought to rough vacuum by two 2000 CFM blowers backed by four 400 CFM mechanical pumps. Seven CVI TM-1200 re-entrant cryopumps with LN2 baffles and a nominal pumping speed of 500,000 L/s on air or 240,000 L/s on xenon achieve high vacuum base pressure in the low 10^{-7} to high 10^{-8} Torr range.

Nested Hall Thruster

The X2 is a 10-kW class laboratory model dual-channel nested Hall thruster (NHT) developed at the University of Michigan Plasmadynamics and Electric Propulsion Laboratory under support from the Michigan / AFRL Center of Excellence in Electric Propulsion (MACEEP).[11] The X2 was intended as a technology demonstrator or proof-of-concept to investigate the operational characteristics of NHTs. Multiple channels optimized for different power ranges give the X2 and NHTs in general an extremely wide power throttling range, which can be spanned at high efficiency by selectively sharing operation between channels. The dual-channel configuration provides for three different types of operation at constant power in a single package: high thrust-to-power operation at high current and low voltage in dual-channel operation, high-I_{sp} operation at high voltage and low current on the smaller inner channel, and a compromise medium I_{sp} capability in outer channel operation.[12] Liang noted, referring to work by Jacobson[10] and Spores[30], that "*[a]vailable literature predating the X2 shows mostly conceptual consideration for NHTs with only a single mention of a development effort*."[13] Busek also developed an approximately 6-kW dual channel Hall thruster in the mid-2000s under a SBIR contract.

Both X2 channels share a centrally mounted lanthanum hexaboride cathode, similar to the one used on the H6 Hall thruster,[31] and for these tests are powered from separate power supplies with a shared cathode common. Joint operation of both channels from a single power supply is also possible. The X2 discharge channels are identical in width, length and anode cross-section with a similar magnetic field shape. The thruster body is electrically grounded to the chamber while the anode and cathode float relative to ground with a fixed discharge voltage applied between them. A RC discharge filter consisting of a 220 μF capacitor rated to 800 VDC placed between each anode and the cathode common together with the resistive load of the thruster discharge itself is used to protect the main discharge power supplies and reduce voltage ripple at the thruster during current oscillations.

All operating conditions presented here are part of sets known as "triads". An X2 NHT operating triad consists of three operating conditions: both individual channel operating cases (inner and outer) and the joint dual-channel case. Within a triad other discharge parameters are held constant, including discharge voltage, discharge current density or mass flow density in each channel, and magnetic field settings. In particular both sets of magnets for the inner and outer channels are kept engaged, even when only one channel is operating. The only differences across a triad are which channels receive anode flow and have discharge voltage applied, and the absolute cathode mass flow rate since a constant cathode flow fraction relative to total anode flow is maintained.

Prior work on the X2—Work to date on the X2 has primarily been aimed at constant-power performance measurements on a thrust stand,[12] supported by time-averaged plume diagnostics necessary for decomposition of performance efficiency into physically meaningful sub-efficiencies relating to mass utilization, voltage utilization, and others as part of a standard Hall thruster efficiency architecture.[7], [13], [32] In these prior works Liang also presents a brief discharge current oscillation study noting that at several dual-channel operating conditions the channels share a breathing mode frequency, and in other cases noting that the breathing mode frequency of one channel appears in the power spectrum of the opposite channel. Of particular note, those cases with shared frequency behavior between channels exhibited the largest amplitude current oscillations, ranging from 10-70% of the mean discharge current.

4. Diagnostics

Discharge current sensors

The X2 inner and outer channel discharge currents are monitored using FW Bell NT magnetoresistive sensors. The NT series provides DC-coupled measurements of discharge current sensitive up to 100 kHz with 3500 V isolation. Two NT sensors are used, a NT-15 and NT-25 for the inner and outer channels of the X2, respectively. Both sensors monitor current to the anode on the thruster side of the discharge filter and are powered off a linear 15 V power supply. The NT-25 has a maximum slew rate of 7.1 A/μs, and the NT-15 has a maximum slew rate of 16.7 A/μs. Neither limit is closely approached in these tests.

Voltage sensors: compensated voltage dividers

For the 250 V triad, X2 inner and outer channel discharge voltages and the cathode floating voltage are recorded. Thruster discharge voltages are of order several hundred volts. This voltage is far too large to pass directly into a data acquisition unit. Passive compensated probes, also known simply as oscilloscope probes, are used to reduce these large voltages while maintaining excellent frequency response. A trimming capacitor on each device is used to match total impedance for DC as well as oscillatory signals. Since these probes must have one end grounded, it is not possible to record the entire anode-to-cathode voltage difference with a single probe – Hall thrusters are operated floating with respect to electrical ground to monitor the health and stability of the cathode discharge through its floating potential.[33] Instead an Avex Electronics Corporation API series 500-100-2 100X voltage divider probe is used to measure anode floating potential (two identical probes are used in dual-channel mode), and an Agilent N2863B 10X divider is used to measure cathode floating potential. These voltages are measured from sense lines on the thruster side of the discharge filter; the sense lines are directly connected to each electrode at the back of the thruster. Both signals are recorded and the difference is computed in postprocessing as the discharge voltage; both discharge voltage and cathode floating potential are both reported.

High-speed Imaging

Measurements of discharge current(s) and voltage(s) in the X2 are supplemented by a high-speed camera imaging the full thruster discharge channel at nearly 100,000 frames per second. The camera is a Photron SA5 FASTCAM with a Nikon ED AF Nikkor 80-200mm lens at its maximum aperture f/2.8. The SA5 is capable of full megapixel 1024x1024 resolution with 12 bits per pixel at up to 7,000 frames per second (fps), with a peak framerate over 1,000,000 fps at 128x16 pixel resolution. All high-speed video shown here was acquired at 87,500 fps with 256x256 pixel resolution, with the exception of the 150V inner channel (single-channel) video at 175,000 fps and 128x128 pixel resolution. For all videos the Nyquist frequency of the framerate is well above the breathing mode (the highest frequency of interest), which peaks below 30 kHz. The 1:1 aspect ratio (square image) is best for Hall thruster imaging to capture the entire discharge channel and make unambiguous identification of rotating instabilities.

The FASTCAM views the thruster axially through a quartz viewport from approximately 6.5 meters downstream. In the horizontal plane (parallel to the ground) the viewport is above thruster centerline and all video is filmed from approximately 2.5 degrees above level. In the vertical plane (perpendicular to ground) the angle varies depending on the thruster position

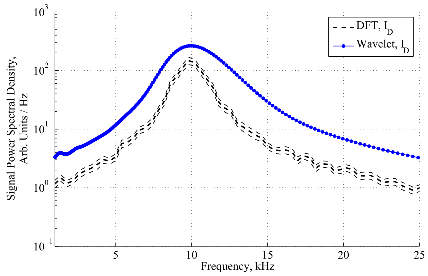

Figure 4. Comparison of discrete Fourier transforms of a X2 discharge current signal to a smoothed version generated from averaging a discrete wavelet transform. The smoothed version is used to estimate discharge current frequency peaks.

but is never more than 20 degrees off-center. Fourier analysis techniques described by McDonald are applied to the video to determine breathing and spoke mode frequencies.[23], [26] FASTCAM video acquisition is triggered from an externally applied 5 VDC signal to synchronize imaging with other data acquisition.

Data Acquisition (DAQ) Devices

A General Standards PMC66-16AISS8AO4 16-bit 8-channel analog input data acquisition card with 8 simultaneously sampled analog-to-digital converters, one per channel, takes samples at between 400 kHz and 1 MHz across both X2 triads. It acquires discharge current measurements from the FW Bell NT sensors and discharge voltage and cathode floating voltage measurements from the passive compensated probes. The card is triggered from an externally applied 5 VDC signal to synchronize data acquisition with FASTCAM video.

5. Data Analysis Techniques

Frequency Analysis

Two techniques are used to analyze frequency content of the thruster discharge current and voltage signals. The first, Fourier analysis, is well-known. We use the built-in *fft* function in MATLAB to compute raw power spectral density (PSD) plots for discharge current, discharge voltage and cathode floating voltage. Since the PSD is often very noisy, we further smooth it by chopping it into discrete frequency bins, assuming the PSD values in that bin are normally distributed, and computing a mean and 95% confidence interval assuming the standard distribution for each frequency bin. Frequency bins are 200 Hz wide from 0 - 10 kHz, 250 Hz wide from 10 - 30 kHz, and 500 Hz wide above 30 kHz. Both the mean and upper and lower confidence bounds are plotted for each signal, with the confidence bounds shown in the same color. For most cases the confidence interval lies sufficiently close to the mean that the three lines appear as a single thick line on the plot. This technique is effective at clearly identifying structure in the frequency content of a signal and identifying qualitative changes in frequency peak location across different operating conditions.

For quantitative comparisons of changes in frequency peaks across different operating conditions, smoothed Fourier PSDs with confidence intervals are not as well-suited. In some cases a clearly peaked PSD presents an obvious answer, but in the case of frequency peaks in the PSD with a large full width at half-maximum (FWHM), noise in the

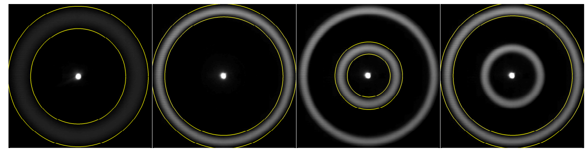

Figure 5. Automated identification of the discharge channel in high speed video of each operating condition across an X2 triad. From left, identification of the inner channel and outer channel in single channel and dual-channel operation.

PSD can throw off identification of the peak by several kilohertz. Instead we use a technique of periodogram averaging that leverages a wavelet transform to maximally average the PSD at each frequency and produce a smooth frequency spectrum with an unambiguous peak. The wavelet transform sacrifices some frequency resolution (note the larger FWHM in Figure 4 for the wavelet compared to the Fourier transform), but it visually preserves the peak location reasonably well and more importantly is repeatable and consistent. Code for the wavelet transform published by Torrence and Compo is used and is freely available at http://paos.colorado.edu/research/wavelets/.[34]

Frequency Analysis - Video

High-speed video is primarily useful for identifying rotating spoke presence and quantifying oscillation frequencies. Thus, the azimuthal variation in image brightness around the Hall thruster channel is far more interesting than the radial dependence. This radial dependence is collapsed by dividing the thruster into azimuthal pie-slice-shaped bins and computing an average pixel brightness versus time every few degrees around the discharge channel. The resulting "spoke surface" is amenable to a 2D Fourier analysis to reveal both unified oscillations of the entire image with time (i.e., the breathing mode) as well as propagating wave structures (the spokes). A detailed procedure for this frequency analysis is given by McDonald.[23], [26]

Some improvements have been made to this technique, including updating the circle-fitting algorithm to be fully automated for a given thruster. The automated fits used to identify the channel region for analysis for each condition of the X2 operating triad are shown below, highlighted in yellow (Figure 5). The discharge channel is divided into 2-degree segments for 180 bins of azimuthal resolution. In all cases the videos are checked for both clockwise and counter-clockwise rotating spoke modes, and in all cases the spokes are found propagating in the $E \times B$ direction.

6. Results and Discussion

We present results from two complete triads, one at 150 V and 3.6 kW total power (6.6 A inner channel, 16.8 A outer channel) and the other at 250 V and 8.6 kW total power (10 A inner channel, 24.6 A outer channel). In the 150 V triad the magnetic field settings were optimized on a thrust stand to maximize thrust at a constant anode flow rate, and an identical mass flow density was maintained on each channel. In the 250 V triad the magnetic field settings were chosen to minimize discharge current for a constant anode flow rate, and an identical discharge current density was maintained across each channel. Cathode flow fractions differed between triads: 10% for the 150 V triad and 7% for the 250 V triad. Also, data for these two triads were taken several months apart,

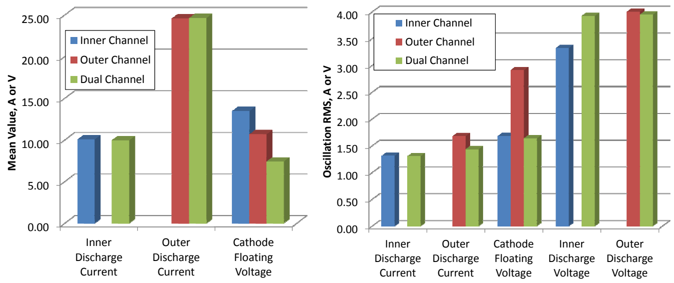

Figure 6. Mean discharge current I_D and cathode floating potential V_{cg} (above), and RMS I_D, V_{cg} and discharge voltage V_D (below) for the 250 V triad

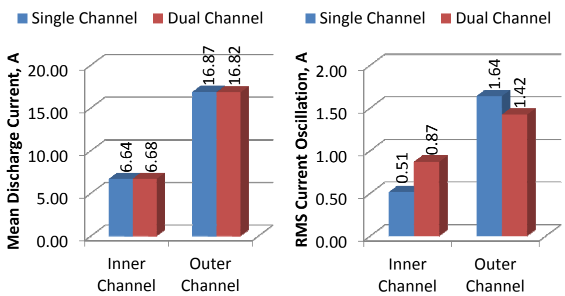

Figure 7. Mean discharge currents I_D (left) and RMS values (right) for the 150 V triad

and in the interim the LaB6 thermionic insert in the hollow cathode was replaced. This caused some changes to operating parameters during the first few tests after replacement but at the time of the data acquired here is not believed to have had an effect.

Discharge Current and Voltage Oscillation Amplitudes

Discharge current(s), discharge voltage(s) and cathode floating voltage were monitored at each 250 V triad operating condition, and discharge current(s) were monitored at each 150 V triad condition. The results are presented in Figures 6 and 7. In general, little change in either the mean or oscillatory components of each channel's operation were observed.

At 250 V the mean discharge currents were essentially constant between single- and dual-channel operation, changing from 10.06 A to 9.95 A on the inner channel and 24.59 A to 24.63 A on the outer channel during single- and dual-channel operation, respectively. These changes of 1% or less for each channel between single and dual channel operation are comparable or less than the 1-2% changes observed at any given operating condition across different test days and pumpdowns. The cathode coupling voltage decreased steadily in magnitude (i.e., moved closer to ground) from -13.5 V for inner channel operation to -10.7 V on the outer channel and -7.4 V for dual-channel operation, likely due to increased absolute cathode flow under the fixed relative cathode flow fraction across conditions. Discharge current RMS oscillations changed from 1.31 A to 1.30 A on the inner channel and 1.68 A to 1.44 A on the outer channel going from single- to dual-channel operation. As a percentage of mean discharge current, the inner channel RMS oscillations were steady at 13% while the outer channel oscillations decreased from 7% to 6% from single- to dual-channel operation.

At 150 V the mean discharge currents again stayed essentially constant across the triad, changing from 6.64 A to 6.68 A on the inner channel and 16.87 to 16.82 A on the outer channel going from single-channel to dual-channel operation. The RMS currents changed more noticeably, increasing from 0.51 A to 0.87 A on the inner channel and decreasing from 1.64 A to 1.42 A on the outer channel. As a percentage of mean discharge current, the oscillations increased from 8% to 13% on the inner channel and decreased from 10% to 8% on the outer channel going from single-channel to dual-channel operation.

Across both cases, peak-to-peak discharge currents captured over the course of a full second of data acquisition ranged from approximately 10-15 times the measured RMS current, or from about 75% to 140% of the mean discharge current. These values raise the question of what is an "acceptable" level of oscillation in the Hall thruster discharge current. For comparison, the Aerojet BPT-4000 is the highest power thruster flight-qualified to date (4.5 kW) and at its nominal 300 V, 15 A operating condition exhibited oscillations with an RMS current of 1.09 A and peak-to-peak oscillations of 14.24 A during ground testing at JPL, for a RMS/mean ratio of 7% and a peak/mean ratio of 95%.[35] The values observed in the X2 are slightly but not appreciably higher than those of the BPT-4000, but it should also be noted that these X2 operating conditions were not tuned in any way to minimize oscillations, and that "quieter" oscillations can probably be found, if necessary.

Discharge Current, Voltage, and Rotating Spoke Oscillation Frequencies

Discharge Current and Voltage Measurements—Peak oscillation frequencies in the X2 in general changed slightly when moving from single- to dual-channel operation in a triad. In the 250 V triad discharge current as well as discharge voltage and cathode floating voltage were monitored, while in the 150 V triad only discharge current was recorded. Frequency spectra for the 250 V case are shown in Figures 8 and 9, while the breathing mode frequencies for both triads are collected in Figure 10. Note that for both triads, separate power supplies powered each anode while sharing the cathode common ground. However, operation at identical operating conditions (mass flow rates, magnet currents and discharge voltages) with separate and shared power supplies has demonstrated little effect on frequency spectra in the X2.[12]

At 250 V in single-channel operation the inner channel exhibits a more sharply peaked breathing mode than the outer channel (Figure 8), and in both cases the cathode floating potential and the discharge voltage follow the discharge current spectrum closely. In the dual channel case there is little change, though it is interesting to note that the cathode floating potential does not clearly follow either channel's spectrum. Since the cathode common is shared between channels, it makes sense that it ought to exhibit a mix of oscillations.

In the 150 V triad (Figure 9) the breathing mode is strongly peaked in each channel in both single- and dual-channel operation, and the outer channel partially couples into the inner channel during dual-channel operation. This is the most clearly noticeable coupling effect of the experiment. Previous X2 results by Liang under dual-channel, constant-power operation showed two types of coupling behavior, which we label "full coupling" and "partial coupling", and the observed behavior in this set of experiments at 150 V falls in the latter category.[12] Under full coupling, both channels

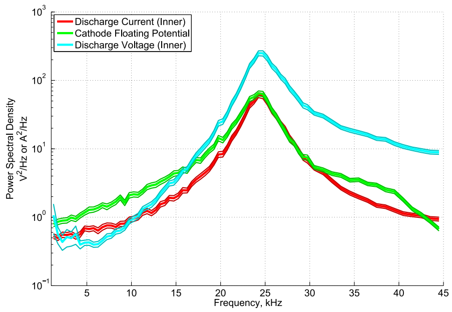

(a) Inner channel operation, 250 V

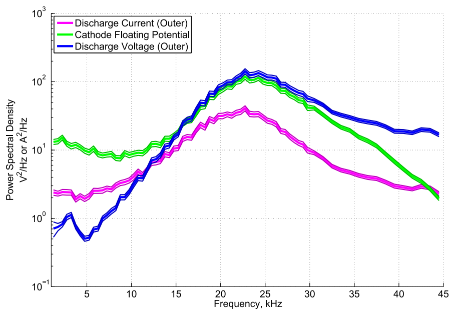

(b) Outer channel operation, 250 V

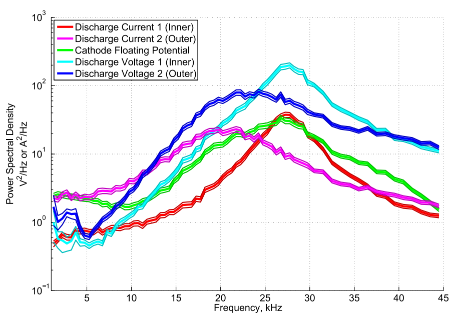

(c) Dual channel operation, 250 V

Figure 8. 250V triad power spectral density for discharge current(s), discharge voltage(s) and cathode floating voltage. The discharge frequency peaks in dual-channel operation bifurcate slightly from their single-channel peaks, as the inner channel frequency increases and the outer channel frequency decreases.

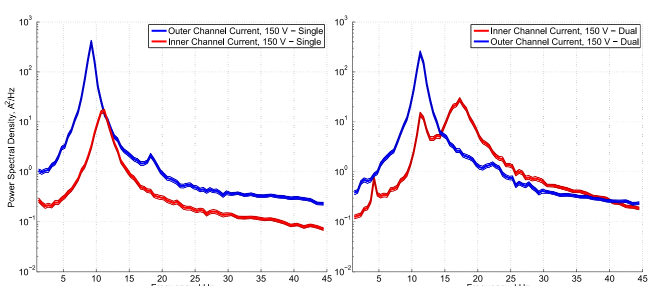

Figure 9. 150V triad power spectral density for single-channel operation discharge currents (left) and dual-channel operation discharge currents (right). Both channels' frequency peaks increase in dual-channel operation, the inner channel by more. Partial coupling occurs with the 11 kHz outer channel breathing mode in (b). The small peak at 4 kHz is a strong spoke mode (see Figure 12b).

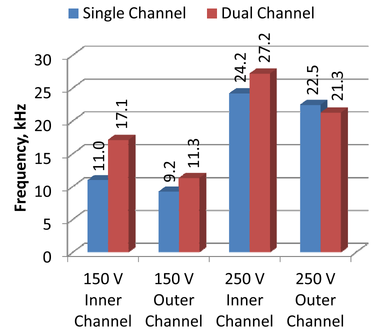

Figure 10. Discharge Current Oscillation Frequencies, X2 150 V and 250 V Triads

exhibit nearly identical frequency spectra, indicating pure joint oscillation of both channels at a single main breathing mode frequency. Liang showed this behavior at 6-kW constant power at discharge voltages of 125 V, 150 V and 350 V (note that constant power-optimized operation is distinct from the triad cases seen here; see Liang for more detail). Under partial coupling, the two channels exhibit distinct frequency spectra with different breathing mode frequencies, but one channel's breathing mode peak shows up as a smaller peak in the other's discharge current spectrum. At 6-kW constant power operation Liang found that the inner channel breathing mode bled into the outer channel's spectrum at 250 V, while at 300 V the reverse occurred.

Full coupling between channels was not observed in these experiments in either triad, but under the partial coupling in the 150 V triad the outer channel breathing mode at about 11 kHz appears on the inner channel as well, indicating that it is bleeding into the inner channel and causing the two to share some oscillations. The strange peak at about 4 kHz on the inner channel observed during dual-channel operation is actually a strong $m = 2$ spoke mode and can be seen clearly later in Figure 12.

Recalling the RMS oscillation levels from Figures 6 and 7, the inner channel RMS current oscillation was steady from single- to dual-channel at 250 V and increased at 150 V, and in the outer channel the RMS current decreased from single- to dual-channel operation in both triads. The partial discharge coupling seen in the 150 V triad suggests that some of the reduction in outer channel oscillation amplitude may be because the outer channel is under a heavier load as it also drives oscillations at its fundamental frequency in the inner channel. In the 250 V triad where no frequency domain coupling was observed, the reduction of the outer channel RMS from 1.68 A to 1.44 A is not associated with any change in the inner channel RMS.

Slight changes in the discharge current oscillation frequencies collected in Figure 10 show no clear trend in transitioning from single- to dual-channel operation. What is surprising about both cases is that during dual-channel operation these fundamental frequencies become farther apart, rather than merging into a single, unified oscillation at a shared frequency. At 150 V the frequency of both channels increases, just by much more in the inner channel case, while in the 250 V case the inner and outer channel frequencies bifurcate, as the inner channel frequency rises and the outer channel frequency lowers. Even in the case of the "shared" 11 kHz oscillation at 150 V from the outer channel influencing the inner channel, the oscillation did not dominate over the inner

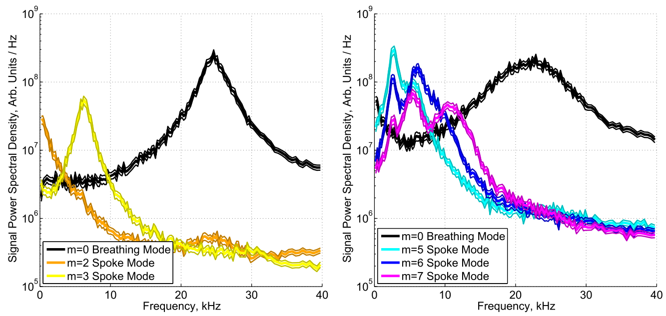

(a) Individual channel 250 V operation for the inner channel (left) and outer channel (right)

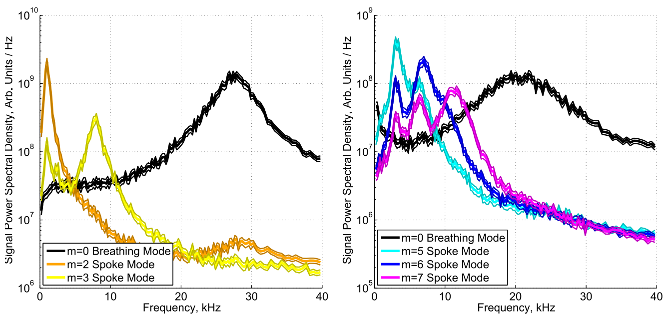

(b) Dual-channel 250 V operation for the inner channel (left) and outer channel (right)

Figure 11. Video DFTs show spoke and breathing mode oscillations across the X2 250 V operating triad. The overall structure of the oscillations is consistent from single- to dual-channel operation. Slight changes in the spoke frequencies are shown in Figure 14.

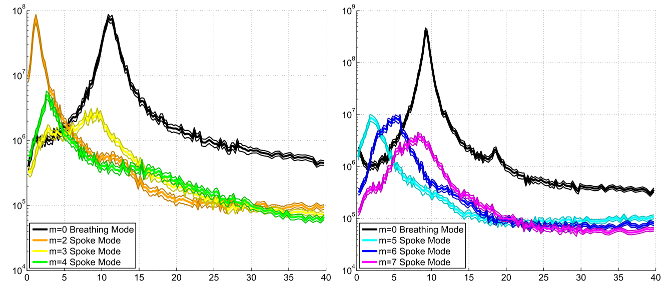

(a) Individual channel 150 V operation for the inner channel (left) and outer channel (right)

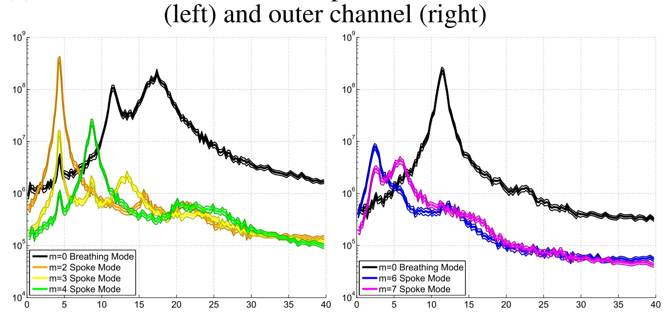

(b) Dual-channel 150 V operation for the inner channel (left) and outer channel (right)

Figure 12. Video DFTs show spoke and breathing mode oscillations across the X2 150 V operating triad. Peak frequencies are tabulated in Figure 14. The very strong $m = 2$ peak on the inner channel during dual-channel operation is also visible in the discharge current frequency spectrum in Figure 9.

channel fundamental frequency.

High-Speed Imaging of Rotating Spokes—a

Frequency analysis of high-speed video are shown for both triads in the following figures. Spectra for breathing and spoke modes are given and denoted by the mode number m; $m = 0$ represents the breathing mode and $m \geq 1$ represents the spoke modes. Mathematically, the $m = 0$ mode represents changes in total image intensity, e.g., oscillations of all image pixels in unison corresponding to brightening or dimming of the entire thruster channel, and is thus an excellent proxy for discharge current oscillations which also tend to produce bursts of visible light around the entire channel due to ionization and excitation. The $m \geq 1$ modes represent pulses propagating azimuthally around the discharge channel, where the value of m indicates how many simultaneous excitations propagate as part of a structure. Still frames of an $m = 3$ mode propagating are shown in Figure 13 for illustration.

Power spectral density for spoke modes $m \geq 1$ are shown only for modes which are greater in magnitude than the breathing mode at their peak frequency. For the X2 these modes are $m = 2$ and $m = 3$ on the inner channel and $m = 5$, 6 and 7 on the outer channel (Figure 11). This follows a general trend that in physically larger thrusters, higher excited spoke modes appear, with most spoke modes falling in a particular band of wavelengths. All of the above X2 modes have wavelengths from 12-18 cm. This is also in the approximate wavelength range observed previously in the H6 Hall thruster.[24]

The widely different spoke frequencies for each thruster and channel nevertheless correspond to a rather narrow range of linear velocities. In all cases this velocity is on the order of a few hundred to a few thousand meters per second, well below the $E \times B$ velocity in the discharge channel (typically ~10^4-10^6 m/s). The velocity v_m of mode m is given by[23]

$$v_m = \frac{2\pi R f_m}{m} \tag{1}$$

where R is the thruster mean channel radius and f_m is the frequency of the m^{th} mode. In Figure 11 several peaks are sometimes present for a given mode; the peak of interest is always the largest peak that is dominant at its frequency. For example, in the outer channel cases the $m = 6$ and $m = 7$ modes have peaks at the same frequency as the $m = 5$ mode. This is an artifact of the Fourier decomposition, causing the nonlinear oscillation at $m = 5$ to have several additional terms in its Fourier representation, just as a sawtooth wave at a given frequency can be Fourier decomposed into an infinite number of sinusoidal modes.

Spoke velocity increases for most observed modes when going from single channel to dual-channel operation (Figure 14), with the exception of the 150 V outer channel case where they decrease. The $m = 5$ mode was not observed in the outer channel during dual channel operation. Error bars for the velocities are computed assuming an uncertainty of ± 1 frequency bin in identifying the frequency peak in the smoothed power spectra of Figure 11, with the exception of the $m = 3$ mode in the 150 V inner channel case where the

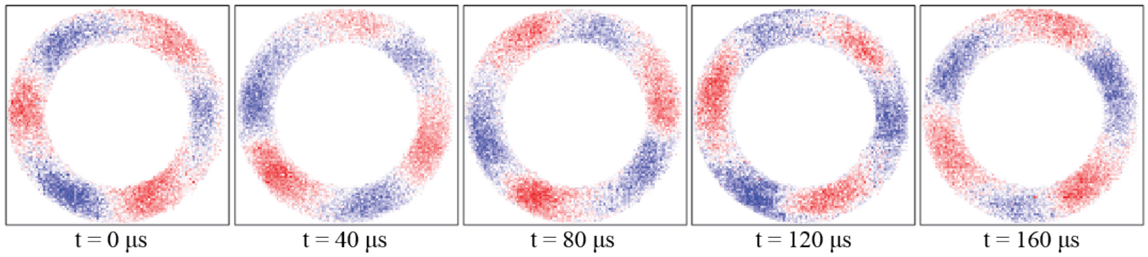

Figure 13. Postprocessed high-speed video still frames showing an example of an spoke mode propagating in a Hall thruster channel. The frames are AC-coupled by subtracting off a mean image taken over tens of thousands of frames and then cast in false color such that brighter-than-average pixels are shown in red and dimmer-than-average pixels are shown in blue. The mode number m=3 denotes the three red regions propagating azimuthally in a coherent structure.

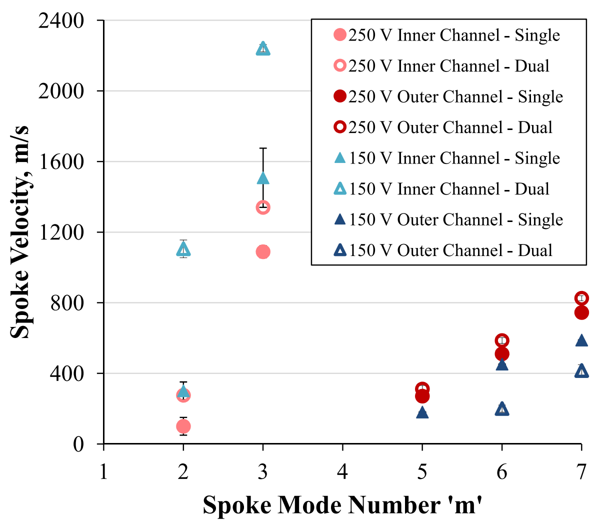

Figure 14. Linear velocities for all clearly identifiable spoke frequencies across both X2 triads

frequency peak was less clear. The velocity error is larger for lower spoke modes m according to Eqn. 1.

The coupling between the inner and outer channels noted in the discharge current spectra previously shown in Figure 9 is again evident in Figure 12b, since the $m = 0$ mode is an excellent proxy for the discharge current. The only electrical coupling in the discharge circuit between channels is due to their shared cathode common, so the fact that the $m = 0$ mode (which measures oscillations of visible light intensity in the discharge channel near the anode) also shows this frequency peak supports the hypothesis that direct coupling between the two channels is taking place in the plasma, as opposed to an electrical circuit effect.

The very strong $m = 2$ mode in the inner channel at 150 V also displays another artifact of the Fourier transform, the appearance of higher harmonics. The $m = 4$ mode is shown in Figure 12 because it displays the second harmonic of the $m = 2$ mode at a frequency $f_4 = 2f_2$. This harmonic further bleeds into the spectrum of the $m = 3$ mode in the dual channel case. In all cases the velocities identified in Figure 14 are calculated from the primary peaks associated with a given mode, and harmonics and other artifacts are not shown.

Triad Voltage	Operating Channel(s): Inner	Outer	Dual
150 V	4.3×10^{-6}	1.1×10^{-5}	1.5×10^{-5}
250 V	6.3×10^{-6}	1.6×10^{-5}	2.2×10^{-5}

Table 1. Calculated chamber background pressure (Torr, corrected for xenon)

Chamber Background Pressure and Neutral Density Effects

Brown linked operating mode transitions in the H6 Hall thruster (see Section 2) at low voltage (100 - 120 V) to neutral density levels in the cathode exit region on thruster centerline driving an undetermined instability[27] by triggering the transition with a variety of methods, including raised chamber background pressure by selective operation of cryopumps, increased cathode flow rates, and flow through an auxiliary port near the cathode. The similar effects observed with all methods localized the region of influence of the elevated neutral flow to the cathode region but indicated that it was caused by phenomenon external to the cathode insert plasma. This section notes changes in background pressure across triad testing and similarities between Brown's auxiliary flow near the cathode and dual channel NHT operation.

During the X2 triad tests chamber base pressure was recorded (approximately 3×10^{-7} Torr for all tests), but operating pressure was not explicitly noted. However, operating pressures recorded in the same facility and in the same period during other X2 and H6 experiments from an externally mounted hot-cathode ion gauge place the effective facility pumping speed at approximately 230,000 L/s, within measurement error of the nominal 240,000 L/s speed of the facility. Table 1 reports calculated facility background pressures corrected for xenon using this effective speed and the total flowrate (anode plus cathode) at each X2 triad condition. From single to dual channel operation the background pressure increased 3.5X; from outer to dual channel the increase was about 40%. The ~30% lower total flowrate in the 150 V triad gives lower pressures for that voltage.

No large Brown-like transitions (i.e., changes of several amperes in RMS current oscillations) were observed under these changes in background pressure. Brown reported transitions in the H6 at pressures in the range of 1 - 4 $\times10^{-5}$ Torr for discharge voltages of 105-120 V.[36] If Brown's hypothesis that transitions occur at lower background pressure with higher discharge voltage is correct, background pressures in the mid-10^{-6} Torr may already be above the threshold for instability of the X2 inner channel at 150 V. However, this is highly speculative, and at present there is no clear analytical description of the instability mechanism describing such transitions to place such a threshold with any certainty, or even to say if such thresholds are primarily a function of discharge voltage, thruster model, facility, cathode placement or other factors.

We nevertheless note that the ~15% reduction in RMS oscillation current on the outer channel going from single- to dual-channel operation in both triads is similar in direction if not in magnitude to the effect observed by Brown when increasing cathode flow fraction or auxiliary neutral flow near the cathode in the H6. Between outer-channel and dual-channel operation the inner channel flow and potential are turned on and the cathode flow increases by ~40% to maintain the overall cathode flow fraction. No attempt was made to isolate how much of this reduction was due to the cathode flow rate change versus the newly operating inner channel in dual-channel mode.

7. Summary and Conclusions

Inter-channel discharge coupling was investigated in the X2 dual-channel nested Hall thruster (NHT) by monitoring discharge current and voltage oscillations and high-speed video to characterize breathing mode and rotating spoke mode oscillation frequencies and amplitudes. These measurements were taken at two sets of so-called "triad" operating conditions corresponding to both individual single-channel operating cases as well as the dual-channel condition of the X2. Within a triad the discharge voltage, anode mass flow rates, cathode flow fractions, and magnetic field settings are constant across operating conditions, and either discharge current density or mass flow density are maintained as well. Only which channels receive anode flow, which channels are biased to the discharge voltage, and the absolute cathode flow vary.

Within triads only minor changes in discharge current oscillation amplitudes and frequencies were observed moving from single- to dual-channel operation. As a percentage of the mean discharge current, at a 150 V, 3.6 kW triad the inner channel RMS oscillations increased from 8% to 13% and outer channel RMS oscillations decreased from 10% to 8% going from single- to dual-channel operation. At a 250 V, 8.6 kW triad the inner channel RMS oscillations stayed steady at 13% and the outer channel oscillations decreased from 7% to 6%. Mean discharge parameters were not noticeably affected with the exception of the cathode floating potential, which increased in magnitude below ground with decreasing absolute cathode flow rate.

A previously reported trend that rotating spoke linear velocity increases with mode number m was confirmed in both channels of the X2 and across both triads. The spoke linear velocity generally increased during dual-channel operation, with the exception of the outer channel at 150 V. In all cases the wavelengths of spoke modes observed in the X2 (either channel) ranged from about 12-18 cm.

For both triads tested, dual-channel operation did not noticeably destabilize the discharge. Full inter-channel coupling, defined as completely shared discharge current frequency spectra in dual-channel operation, was not observed at either triad. Partial coupling, defined as weaker appearance of frequency peaks from one channel's spectrum superimposed on the opposite channel's spectrum, was observed at the 150 V triad. In the 150 V case the outer channel breathing mode frequency influenced the inner channel and appeared in both discharges, causing at least in part the slightly elevated RMS oscillation levels noted above. These levels are comparable or slightly higher than reported values for the BPT-4000 flight-qualified Hall thruster, and are not considered problematic. Neither triad was tuned to reduce oscillations in any way. The overall similarity of NHT channel operating characteristics whether operated singly or in the multi-channel configuration is encouraging for ease of laboratory testing and further development of the technology.

Acknowledgments

A portion of this research was carried out at the Jet Propulsion Laboratory, California Institute of Technology, under a contract with the National Aeronautics and Space Administration and funded through the Director's Research and Development Fund program. The first author gratefully acknowledges support under this funding during the period this research was performed. The second author acknowledges support during this work by a NASA Office of the Chief Technologist Space Technology Research Fellowship. The Plasmadynamics and Electric Propulsion Laboratory (PEPL) at the University of Michigan is supported under the Michigan / AFRL Center of Excellence in Electric Propulsion (MACEEP) under contract monitor Mitat Birkan. Special thanks also go to PEPL doctoral candidate Ray Liang, without whose expertise, training and gracious assistance in operating the X2 (to say nothing of his design and construction of it in the first place), this work would not have been possible.

References

[1] J. Brophy, R. Gershman, N. Strange, D. Landau, R. Merrill, and T. Kerslake, "300-kW solar electric propulsion system configuration for human exploration of near-earth asteroids," in *47th AIAA/ASME/SAE/ASEE Joint Propulsion Conference & Exhibit*. AIAA-2011-5514, 2011.

[2] "Fast access spacecraft testbed (FAST)," Defense Advanced Research Programs Agency (DARPA), Tactical Technology Office, Broad Agency Announcement BAA 07-65, 2007.

[3] M. Breen, A. Streett, D. Cokin, R. Stribling, A. Mason, and S. Sutton, "IBIS (Integrated Blanket/Interconnect system), Boeing's solution for implementing IMM (Inverted metamorphic) solar cells on a light-weight flexible solar panel," in *2010 35th IEEE Photovoltaic Specialists Conference (PVSC)*, Jun. 2010, pp. 000 723 – 000 724.

[4] M. T. Maybury, "Energy horizons: A science and technology vision for air force energy," *Air and Space Power Journal*, vol. 26, no. 2, pp. 3–30, Apr. 2012.

[5] D. Brown, B. Beal, and J. Haas, "Air force research laboratory high power electric propulsion technology development," in *IEEE Aerospace Conference*, 2010, pp. 1 –9.

[6] D. Manzella, R. Jankovsky, and R. Hofer, "Laboratory model 50 kW hall thruster," in *38th AIAA/ASME/SAE/ASEE Joint Propulsion Conference*

& Exhibit. AIAA-2002-3676, Jul. 2002.

[7] R. R. Hofer, "Development and characterization of high-efficiency, high-specific impulse xenon hall thrusters," Ph.D. dissertation, University of Michigan, 2004.

[8] N. Strange, R. Merrill, D. Landau, B. Drake, J. Brophy, and R. Hofer, "Human missions to phobos and deimos using combined chemical and solar electric propulsion," in *47th AIAA/ASME/SAE/ASEE Joint Propulsion Conference & Exhibit*, Jul. 2011.

[9] R. Hofer and T. Randolph, "Mass and cost model for selecting thruster size in electric propulsion systems," in *47th AIAA/ASME/SAE/ASEE Joint Propulsion Conference & Exhibit*. AIAA-2011-5518, Jul. 2011.

[10] D. T. Jacobson, J. W. John, H. Kamhawi, D. H. Manzella, and P. Y. Peterson, "An overview of hall thruster development at NASA's john h. glenn research center," in *41st AIAA/ASME/SAE/ASEE Joint Propulsion Conference & Exhibit*. Tucson, AZ: AIAA 2005-4242, Jul. 2005.

[11] R. Liang, "The combination of two concentric discharge channels into a nested hall-effect thruster," Ph.D. dissertation, University of Michigan, Ann Arbor, MI, 2012.

[12] R. Liang and A. D. Gallimore, "Constant-power performance and plume measurements of a nested-channel hall-effect thruster," in *32nd International Electric Propulsion Conference*. Wiesbaden, Germany: IEPC 2011-049, 2011.

[13] R. Liang and A. Gallimore, "Far-field plume measurements of a nested-channel hall-effect thruster," in *49th AIAA Aerospace Sciences Meeting*. AIAA-2011-1016, Jan. 2011.

[14] R. F. Florenz and A. D. Gallimore, "Developmental status of a 100-kW class laboratory nested channel hall thruster," in *32nd International Electric Propulsion Conference*. IEPC-2011-246, 2011.

[15] R. Florenz, T. M. Liu, A. D. Gallimore, H. Kamhawi, D. L. Brown, R. R. Hofer, and J. E. Polk, "Electric propulsion of a different class: The challenges of testing for MegaWatt missions," in *48th AIAA/ASME/SAE/ASEE Joint Propulsion Conference & Exhibit*. AIAA-2012-3942, Aug. 2012.

[16] E. Y. Choueiri, "Plasma oscillations in hall thrusters," *Physics of Plasmas*, vol. 8, no. 4, p. 1411, 2001.

[17] J. M. Fife, M. Martinez-Sanchez, and J. Szabo, "A numerical study of low-frequency discharge oscillations in hall thrusters," in *33rd AIAA/ASME/SAE/ASEE Joint Propulsion Conference & Exhibit, Seattle, WA*. AIAA-1997-3052, 1997.

[18] J. P. Boeuf and L. Garrigues, "Low frequency oscillations in a stationary plasma thruster," *Journal of Applied Physics*, vol. 84, no. 7, pp. 3541–3554, Oct. 1998.

[19] G. S. Janes and R. S. Lowder, "Anomalous electron diffusion and ion acceleration in a low-density plasma," *Physics of Fluids*, vol. 9, p. 1115, 1966.

[20] D. Liu, R. E. Huffman, R. D. Branam, and W. A. Hargus, "Ultrahigh-speed imaging of hall-thruster discharge oscillations with krypton propellant," *IEEE Transactions on Plasma Science*, 2011.

[21] C. L. Ellison, Y. Raitses, and N. J. Fisch, "Cross-field electron transport induced by a rotating spoke in a cylindrical hall thruster," *Physics of Plasmas*, vol. 19, no. 1, pp. 013 503–013 503–7, Jan. 2012.

[22] J. B. Parker, Y. Raitses, and N. J. Fisch, "Transition in electron transport in a cylindrical hall thruster," *Applied Physics Letters*, vol. 97, no. 9, p. 091501, 2010.

[23] M. S. McDonald and A. D. Gallimore, "Measurement of cross-field electron current in a hall thruster due to rotating spoke instabilities," in *47th AIAA/ASME/SAE/ASEE Joint Propulsion Conference & Exhibit*. AIAA 2011-5810, 2011.

[24] M. McDonald and A. Gallimore, "Parametric investigation of the rotating spoke instability in hall thrusters," in *32nd International Electric Propulsion Conference*. IEPC 2011-242, 2011.

[25] M. S. McDonald and A. D. Gallimore, "Rotating spoke instabilities in hall thrusters," *IEEE Transactions on Plasma Science*, vol. 39, no. 11, pp. 2952–2953, Nov. 2011.

[26] M. S. McDonald, "Electron transport in hall thrusters," Ph.D. dissertation, University of Michigan, Ann Arbor, MI, 2011.

[27] D. Brown and A. Gallimore, "Investigation of low discharge voltage hall thruster operating modes and ionization processes," in *31st International Electric Propulsion Conference*. IEPC 2009-074, 2009.

[28] M. E. Griswold, C. L. Ellison, Y. Raitses, and N. J. Fisch, "Feedback control of an azimuthal oscillation in the e x b discharge of hall thrusters," *Physics of Plasmas*, vol. 19, no. 5, pp. 053 506–053 506–4, May 2012.

[29] M. J. Sekerak, M. S. McDonald, A. D. Gallimore, and R. R. Hofer, "Hall thruster plume measurements from high-speed dual langmuir probes with ion saturation reference," in *2013 IEEE Aerospace Conference*, Big Sky, MT, Mar. 2013.

[30] R. Spores, J. Monheiser, B. P. Dempsey, D. Wade, K. Creel, D. Jacobson, and J. Drummond, "A solar electric propulsion cargo vehicle to support NASA lunar exploration program," in *29th International Electric Propulsion Conference*, 2005, pp. IEPC–2005–320.

[31] D. M. Goebel and R. M. Watkins, "Compact lanthanum hexaboride hollow cathode," *Review of Scientific Instruments*, vol. 81, no. 8, p. 083504, 2010.

[32] D. Brown, C. Larson, B. Beal, and A. Gallimore, "Methodology and historical perspective of a hall thruster efficiency analysis," *Journal of Propulsion and Power*, vol. 25, no. 6, pp. 1163–1177, 2009.

[33] D. F. Hall, R. F. Kemp, and H. Shelton, "Mercury discharge devices and technology," in *AIAA Electric Propulsion and Plasmadynamics Conference*. AIAA-1967-669, 1967.

[34] C. Torrence and G. P. Compo, "A practical guide to wavelet analysis," *Bulletin of the American Meteorological Society*, vol. 79, no. 1, pp. 61–78, Jan. 1998.

[35] R. R. Hofer, D. M. Goebel, J. S. Snyder, and I. Sandler, "BPT-4000 hall thruster extended power throttling range characterization for NASA science missions," in *31st International Electric Propulsion Conference*. IEPC 2009-085, 2009.

[36] D. Brown, "Investigation of low discharge voltage hall thruster characteristics and evaluation of loss mecha-

nisms," Ph.D. dissertation, University of Michigan, Ann Arbor, MI, 2009.

BIOGRAPHY

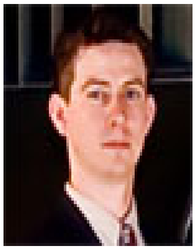

Michael McDonald *received B.S.E. degrees in Aerospace Engineering and Engineering Physics and the Ph.D. degree in Applied Physics from the University of Michigan, Ann Arbor, MI in 2006 and 2011, respectively. He was previously a National Science Foundation Graduate Research Fellow and performed this work as a post-doctoral research scientist at the University of Michigan Plasmadynamics and Electric Propulsion Laboratory. He is currently an Aerospace Engineer in the Naval Center for Space Technology at the US Naval Research Laboratory in Washington, DC. His research interests include high-speed plasma diagnostics, digital signal processing including image processing, low-temperature plasma physics and plasma instabilities, and electric spacecraft propulsion.*

Michael Sekerak *received a B.S. in Mechanical Engineering from Illinois Institute of Technology in 1999 and an M.S. in Aeronautics and an Engineer's Degree from California Institute of Technology in 2001 and 2005, respectively, while conducting research at NASA JPL. He served in the Army as a cavalry officer including one combat tour in Iraq and the Missile Warning Center in Cheyenne Mountain. He is a Major in the Air Force Reserves teaching with the Reserve National Security Space Institute. Prior to the Ph.D. program at University of Michigan, he was an aerospace engineer with the Missile Systems group at Sandia National Laboratories.*

Alec D. Gallimore *is an Arthur F. Thurnau Professor of Aerospace Engineering at the University of Michigan where he directs the Plasmadynamics and Electric Propulsion Laboratory. He received his B.S. in Aeronautical Engineering from Rensselaer, and his M.A. and Ph.D. degrees in Aerospace Engineering with an emphasis in plasma physics from Princeton. His primary research interests include electric propulsion, plasma diagnostics, use of plasma for environmental remediation, and nano-particle physics. He is the author of 300 journal and conference papers on electric propulsion and plasma physics, and is a Fellow of the American Institute of Aeronautics and Astronautics (AIAA).*

Richard Hofer *received the B.S.E. degree in mechanical engineering and the B.S.E., M.S.E, and Ph.D. degrees in aerospace engineering from the University of Michigan, Ann Arbor, MI, in 1998, 1998, 2000, and 2004, respectively. He is a Senior Engineer at the Jet Propulsion Laboratory where he is the technology lead responsible for the development and qualification of Hall thrusters for deep space missions. He is a recognized expert in Hall thruster design, having designed several advanced Hall thrusters ranging in power from 1 to 100 kW. Thruster technology developed by Dr. Hofer is now used in every internal Hall thruster development of the United States Government. In 2011, he received the NASA Exceptional Achievement Medal and the JPL Lew Allen Award for Excellence. Dr. Hofer is an Associate Fellow of the AIAA and a member of the AIAA Electric Propulsion Technical Committee. He has authored over 65 technical publications in the field of electric propulsion.*